Received: 6 March 2017 | Revised: 16 July 2017 | Accepted: 8 August 2017

DOI: 10.1002/cne.24301

RESEARCH ARTICLE

WILEY The Journal of Comparative Neurology

Juxtanodin in retinal pigment epithelial cells: Expression and biological activities in regulating cell morphology and actin cytoskeleton organization

Fengyi Liang[1] | Ji Hyun Hwang[1] | Nicholas Weiwei Tang[1] | Walter Hunziker[2,3,4]

[1]Department of Anatomy, Yong Loo Lin School of Medicine, National University of Singapore, Singapore, Singapore

[2]Epithelial Cell Biology Laboratory, Institute of Molecular and Cell Biology, A*STAR, Singapore, Singapore

[3]Department of Physiology, National University of Singapore, Singapore, Singapore

[4]Singapore Eye Research Institute, Singapore, Singapore

Correspondence
Fengyi Liang, Department of Anatomy, Yong Loo Lin School of Medicine, National University of Singapore, Block MD10, 4 Medical Drive, Singapore 117597.
Email: antlfy@nus.edu.sg

Abstract

Juxtanodin (JN, also known as ermin) was initially identified as an actin cytoskeleton-related oligodendroglial protein in the rat central nervous system. It was subsequently also found in the rat olfactory neuroepithelium, especially at the apical junctional belt of the sustentacular cells. We further examined JN expression and functional roles in the retina using fluorescence histochemistry, confocal microscopy, immuno-electron microscopy, molecular biology, and cell culture. Prominent JN expression was found in the photoreceptor-supporting retinal pigment epithelium (RPE), especially in a zone corresponding to the apices of RPE cells, at the roots of the RPE microvilli, and at the base of RPE cells next to the Bruch's membrane. Partial co-localization of JN immunoreactivity with F-actin (labeled with phalloidin) was observed at the apices and bases of RPE cells. No JN was detected in other cell types of the retina. In cultured human RPE cell line ARPE-19, expression of extrinsic JN up-regulated formation of actin cytoskeleton stress fibers, caused redistribution of more F-actin fibers to the cell periphery, and promoted spreading/enlargement of transfected cells. These findings suggest possible roles of JN in RPE molecular transport, phagocytosis and formation of outer blood-retinal barrier, or possible involvement of JN expression perturbations in pathogenesis of such retinal disorders as proliferative vitreoretinopathy and age-related macular degeneration.

KEYWORDS

actin cytoskeleton, ERM protein, juxtanodin (JN), retinal pigment epithelium (RPE), stress fiber, RRID: CVCL_0145, RRID: AB_476955

1 | INTRODUCTION

Juxtanodin (JN) was originally identified as an actin cytoskeleton-related protein preferentially expressed in oligodendroglia and myelin sheath in the central nervous system (CNS) (Zhang et al., 2005). At sites of myelin–axon interaction, JN is especially enriched in the juxtanodal terminal loops of CNS myelin sheath. At the molecular level, JN shares the C-terminal F-actin-binding domain of ezrin–radixin–moesin (ERM) family proteins. In vitro, JN binding inhibits F-actin depolymerization (Meng, Xia, Tang, Tang, & Liang, 2010). Overexpression of JN protein markedly promotes arborization and intracellular molecular trafficking of cultured oligodendrocyte precursor cells (Meng et al., 2010; Zhang et al., 2005). The mouse homolog of rat JN was subsequently identified and named Ermin, with similar structure and functions (Brockschnieder, Sabanay, Riethmacher, & Peles, 2006).

Outside the CNS, JN was found in the glia-like sustentacular cells of the olfactory epithelium, especially at the roots of sustentacular microvilli and at the tips of the sustentacular apical processes (Tang,

Abbreviations: ABC, avidin-biotinylated horseradish peroxidase complex; AP, alkaline phosphatase; CD11b, integrin alpha M; CNPase, 2′, 3′-cyclic nucleotide 3′-phosphodiesterase; DAPI, 4′, 6-diamidino-2-phenylindole; DMEM, Dulbecco's modified Eagles medium; ERM, ezrin–radixin–moesin; FBS, fetal bovine serum; GFAP, glial fibrillary acidic protein; GST, glutathione S-transferase; JN, Juxtanodin; LSD, least significant difference; MAP2, microtubule-associated protein 2; MBP, myelin basic protein; PB, phosphate buffer; PBS, phosphate buffered saline; ROD, Relative optical density; ROI, region of interest; RPE, retinal pigment epithelium; SIRT2, sirtuin 2; TuJ1-r, neuron-specific class III β-tubulin; ZO1, zonula occludens 1 (tight junction-associated polypeptide).

TABLE 1 List of antibodies

Antibodies against (RRID)	Host	Supplier (Catalog number)	Dilution
CD11b (OX42), IgG, McAb (AB_566455)	Ms	Bio-Rad, Oxford, UK (MCA275GA)	1:50
CNPase, IgG, McAb	Ms	US Biol., Swampscott, MA, USA (352679)	1:200
Ezrin, IgG, McAb (AB_476955)	Ms	Sigma-Aldrich, St. Louis, MO, USA (E8897)	1:2,000
FLAG tag, IgG, PcAb (AB_439687)	Rb	Sigma-Aldrich (F7425)	1:200
GFAP, IgG, McAb (AB_2109815)	Ms	Millipore, Billerica, MA, USA (MAB360)	1:1,000
Juxtanodin (JN), PcAb	Rb	In-house produced (against aa residues 1-170 of rat JN)	1:100
MAP2, IgG, McAb (AB_477256)	Ms	Sigma-Aldrich (M9942)	1:200
MBP, IgG, McAb (AB_240843)	Ms	Millipore (MAB387-1ML)	1:200
SIRT2, IgG, PcAb	Rb	In-house produced, (against aa residues 209-350 of rat SIRT2)	1:200
α-Tubulin, IgG, McAb (AB_477582)	Ms	Sigma-Aldrich (T6074)	1:2,000
Class III β-tubulin (TuJ1), IgG, McAb (AB_2210524)	Ms	Millipore (MAB1637)	1:1,000
ZO1, IgG, McAb (AB_2533147)	Ms	Invitrogen, Carlsbad, CA, USA (33-9100)	1:500
Ms IgG, Alexa Fluor488-conjugated, PcAb (AB_2534069)	Gt	Invitrogen (A-11001)	1:400
Rb IgG, Alexa Fluor568-conjugated, PcAb (AB_143157)	Gt	Invitrogen (A-11011)	1:400
Rb IgG, AP-conjugated, PcAb (AB_11210173)	Gt	Millipore (AP132A)	1:10,000
Ms IgG, AP-conjugated, PcAb (AB_92516)	Rb	Millipore (AP160A)	1:1,000
Rb IgG, Biotin-conjugated, PcAb (AB_2336810)	Gt	Vector Labs, Burlingame, CA, USA (PK-4001)	1:200

Abbreviations: aa, amino acid; AP, alkaline phosphatase; CD11b, integrin alpha M; CNPase, 2′,3′-cyclic nucleotide 3′-phosphodiesterase; GFAP, glial fibrillary acidic protein; Gt, goat; MAP2, microtubule-associated protein 2; MBP, myelin basic protein; McAb, monoclonal antibody; Ms, mouse; PcAb, polyclonal antibody; Rb, rabbit; RRID, Research Resource Identifier; SIRT2, sirtuin 2; ZO1, tight junction-associated polypeptide (Zonula Occludens 1).

Tang, Ling, Wu, & Liang, 2009). This finding of JN in the olfactory epithelium led us to the search for JN-expressing cells in other sensory organs.

Like olfactory sustentacular cells, retinal pigment epithelial cells (RPE cells) also possess long apical microvilli that interdigitate with cone and rod photoreceptor neurons. Here we report specific expression of JN in rat RPE cells, which serve multiple structural and functional roles as epithelial barriers, scavenger and supporting cells for retinal photoreceptor neurons. The RPE cells are important not only in the development, metabolism, molecular trafficking, and structural integrity of retinal photoreceptors, but also in the formation of the outer blood-retinal barrier for the maintenance of the retinal extracellular milieu. Abnormalities in RPE structure, molecular composition or functions have been linked to diverse diseases of the retina such as proliferative vitreoretinopathy and age-related macular degeneration (Chiba, 2014; Plafker, O'Mealey, & Szweda, 2012; Sparrow, Hicks, & Hamel, 2010). The present study investigated JN expression in the retina, and functional roles of JN on morphology and actin cytoskeleton organization of cultured RPE cells.

2 | MATERIALS AND METHODS

2.1 | Experimental animals and antibodies

Fourteen adult rats (Wistar strain, 240–400 g body weight, male or female) were purchased from the National University of Singapore Laboratory Animal Center, and used for the present study. All animal experiments followed strict guidelines or regulations, and were approved by the Institutional Animal Care and Use Committee at the National University of Singapore.

Antibodies used in the present study are listed in Table 1, and are mostly the same as those used to detect JN expression in the olfactory epithelium (Tang et al. 2009). Anti-JN rabbit polyclonal antibody was in-house produced against the glutathione S-transferase (GST)-JN170 (encoding amino acid residues 1–170 of rat JN) fusion protein, and anti-sirtuin 2 (SIRT2) rabbit polyclonal antibody against the GST-SIRT2c (encoding amino acid residues 209–350 of rat SIRT2) fusion protein. The antibodies were then affinity purified by the respective immunogens, and adsorbed by the recombinant GST. Rhodamine-conjugated phalloidin (Catalog #: PHDR1, Cytoskeleton Inc., Denver, CO, USA, 100 nM) was used to mark F-actin on retinal histological sections or cell culture preparations.

2.2 | Antibody characterization

To confirm specificity of the in-house made JN antibody, we compared JN immunoreactivity of the retina/eye with that of the brain on Western blot. The findings are presented in the Results (Section 3.1) and in Figure 1f. Besides, the JN antibody immuno-stained the myelin sheaths and oligodendroglia of the extra-ocular optic nerve, as did the antibody against SIRT2, another marker of CNS myelin sheath (Figures 1c & 3b,e)

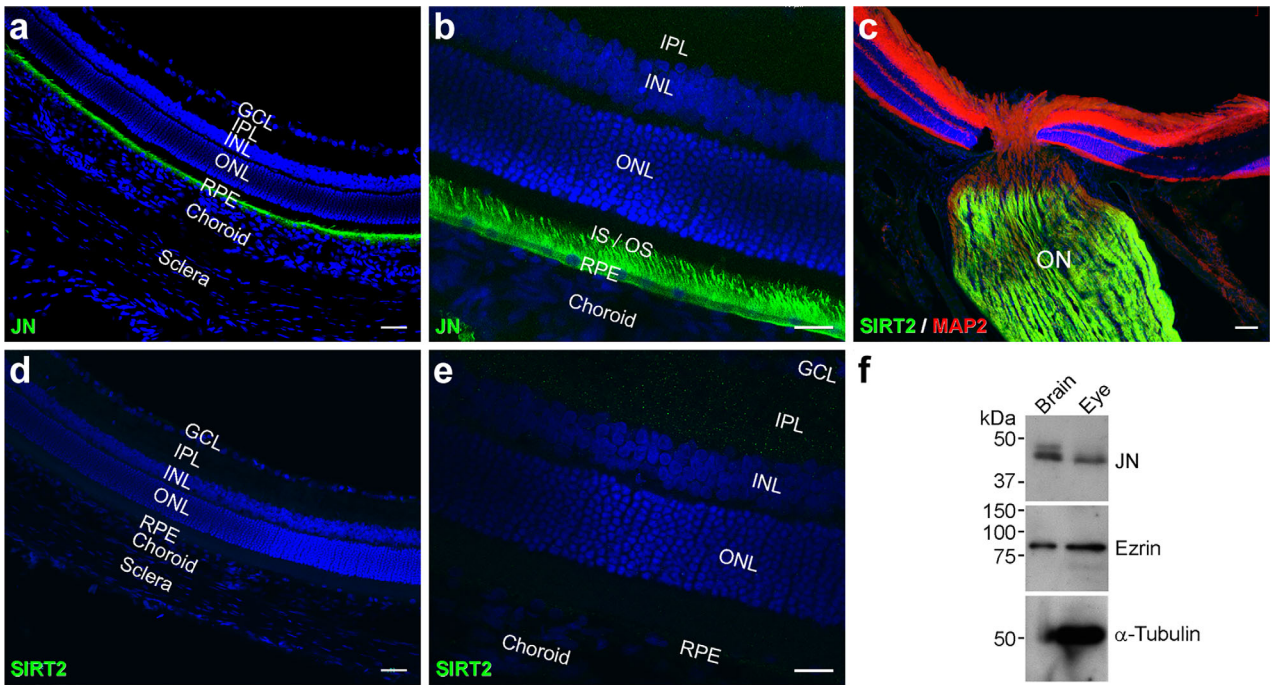

FIGURE 1 JN was found in RPE cells of the retina. (a, b) JN expression was found in the RPE cells of the retina. Note the marked JN signals in the microvilli of RPE cells in panel (b). (c–e) Fluorescence immunohistochemistry revealed no reactivity for SIRT2 in the rat retina (d, e), but prominent SIRT2 signal in the extraocular part of the optic nerve (c). MAP2 immunoreactivity (red) was used to reveal neuronal cell bodies and processes in panel (c). Abbreviations: GCL, ganglion cell layer; INL, inner nuclear layer; IPL, inner plexiform layer; IS/OS, inner/outer segment layer of the photoreceptors; ON, optic nerve; ONL, outer nuclear layer; RPE, retinal pigment epithelium. Scale bars, 40 μm for panels (a, d), 20 μm for (b, e), and 80 μm for panel (c). (f) Western blot confirmed the presence of JN in the eye. The level of JN expression in the eye is similar to that in the brain. Immunoblotting for Ezrin and α-tubulin served as controls

(Li et al., 2007; Zhang et al., 2005). The same JN antibody was also previously characterized on Western blot by comparing brain JN with FLAG-tagged JN overexpressed in cultured cells and revealed by using both the JN antibody and a commercial antibody against FLAG tag. Immunoprecipitation and comparison of immunohistochemical data by using the in-house antibody with data from in situ hybridization histochemistry were also performed (Zhang et al., 2005).

Other antibodies used in the present study (Table 1) have been characterized previously. Immunostainings by these antibodies produced results similar to those previously reported for SIRT2 (Li et al., 2007; Southwood, Peppi, Dryden, Tainsky, & Gow, 2007), CD11b (OX42, RRID: AB_566455), CNPase, FLAG tag (RRID: AB_439687), GFAP (RRID: AB_2109815), MAP2 (RRID: AB_477256), MBP (RRID: AB_240843), α-tubulin (RRID: AB_477582), ZO1 (RRID: AB_2533147) (Zhang et al., 2005; Li et al., 2007; Xia & Liang, 2012), Class III β-tubulin (TuJ1-r, RRID: AB_2210524) (Russo et al., 2011) and ezrin (RRID: AB_476955) (Bonilha, Finnemann, & Rodriguez-Boulan, 1999).

2.3 | Cell culture and transfection

ARPE-19 cell line of human origin was purchased from ATCC (RRID: CVCL_0145, American Type Culture Collection, Manassas, VA). The cells were cultured in Dulbecco's modified Eagles medium (DMEM)/F12 medium (1:1) supplemented with 10% fetal bovine serum (FBS) at 37°C and 5% CO_2. cDNA nucleotide sequences encoding rat JN (282 amino acid residues, Genbank: DQ119821) and JN141 (residues 1–141 of JN) were sub-cloned by polymerase chain reactions into pXJ40 mammalian expression vector with an in-frame FLAG tag at the 5′-end of the insert (Manser et al., 1997; Zhang et al., 2005). The truncated JN141 lacks the C-terminal F-actin binding domain of JN, and has been shown to be devoid of obvious biological activities of JN on primary oligodendroglia precursor cells and OLN-93 oligodendroglia cell line. Here it served as a negative control to JN (Zhang et al., 2005; Meng et al., 2010). Transfection of the cells for transient overexpression of JN or JN141 was carried out by electroporation (3 pulses of 1200 volts, 20-ms pulse duration and 1-s inter-pulse interval) using MP-100 Microporator (Digital Bio Technology, Seoul, South Korea). 1×10^5 cells were mixed with 0.5-μg plasmid DNA in 10-μl resuspension buffer for the electroporation. The cells were then cultured for another 48 hr in the wells of 24-well culture plates before being fixed in 3% paraformaldehyde in 0.1-M phosphate buffer (PB, pH 7.4) at room temperature for 30 min. The level of confluency of the cultured cells was about 60–80% at the time of fixation. The cell culture was washed in 0.01-M phosphate buffered saline (PBS, pH 7.4), and then stained for immunocytochemistry or F-actin cytochemistry (see below).

2.4 | Western blotting

Immunoblotting protocols for JN and other proteins have been described previously (Liang, Wang, Ow, Chen, & Ong, 2017). Briefly,

adult Wistar rats ($n = 2$) were euthanized by decapitation under deep anesthesia and the eye balls were rapidly dissected, together with samples of the brain as positive controls. The tissues were immediately homogenized in T-PER™ tissue protein extraction reagent (Pierce Biotechnology, Rockford, IL). The tissue lysates were assayed for protein content using bicinchoninic acid protein assay kit (Pierce Biotechnology), resolved by electrophoresis (20 μg each) on 12% sodium dodecyl sulfate-polyacrylamide gel (SDS-PAGE), and then electro-transferred onto PVDF (polyvinylidene fluoride) membranes (PerkinElmer, Boston, MA, USA). 5% nonfat milk (Bio-Rad, Hercules, CA) and 0.1% Tween-20 (in 0.01-M PBS, pH 7.4) was used to block non-specific binding prior to overnight incubation at room temperature in the primary antibody (rabbit anti-JN at 1:100, mouse anti-ezrin at 1:2,000, or mouse anti-α-tubulin at 1:2,000 dilution). After washing, the membranes were incubated with alkaline phosphatase-conjugated secondary antibodies (RRID: AB_11210173 or RRID: AB_92516). Immuno-reactive signals were visualized by using CDP-Star chemiluminescence reagent (Roche, Basel, Switzerland).

2.5 | Immunohistochemistry, immunocytochemistry and F-actin histo-/cyto-chemistry

For immunohistochemistry and F-actin histochemistry, adult rats ($n = 10$) were euthanized with an overdose of Nembutal (60 mg/kg of body weight, i.p.), and perfused transcardially with saline followed by a freshly prepared fixative solution of 3% paraformaldehyde in 0.1-M PB (pH 7.4). The eye balls and brain (as positive control) were carefully dissected. The tissues were post-fixed in the same fixative for 3 hr at 4°C, and then cryo-protected in 30% sucrose in 0.1-M PBS (pH 7.4) for 12 hr. The specimens were cut into 30-μm thick sections on a cryostat, thaw-mounted on 2% gelatin-coated glass slides and stored at −20°C.

For fluorescence immunohistochemistry/immunocytochemistry, the histological sections/cultured ARPE-19 cells were rinsed for 3 times with 0.01-M PBS (pH 7.4), and then incubated in PBS-T-NGS (0.3% Triton X-100 and 6% normal goat serum in PBS, pH7.4) for 1 hr at room temperature to block nonspecific reactions. This was followed by overnight incubation at room temperature in the solution of primary antibodies consisting of rabbit anti-JN, rabbit anti-FLAG tag or rabbit anti-SIRT2 (sirtuin 2) plus one of the following mouse antibodies in PBS-T-NGS: anti-ezrin, anti-class III β-tubulin (TuJ1), anti-CNPase (2′, 3′-cyclic nucleotide-3′-phosphodiesterase), anti-MBP (myelin basic protein), anti-MAP2, anti-GFAP (glial fibrillary acidic protein), anti-CD11b (OX42) or anti-ZO1 (tight junction-associated polypeptide, zonula occludens 1). Negative control sections/cell cultures were incubated in parallel in the same PBS-T-NGS buffer without either or both of the primary antibodies. After washes in PBS, the immunoreactivities were visualized by secondary antibodies conjugated to either Alexa Fluor 488 (RRID: AB_2534069) or Alexa Fluor 568 (RRID: AB_143157) (Invitrogen, Carlsbad, CA) that yielded green and red fluorescence, respectively. The sections/cell cultures were finally incubated in 4′,6-diamidino-2-phenylindole (DAPI, 0.2 μg/ml) for 20 min to reveal cell nuclei. After rinses in PBS, the tissue sections/cell cultures were cover-slipped using an aqueous mounting medium (8% gelatin, 50% glycerol & 0.1% NaN_3 in 0.01-M PB, pH 7.4), and observed under a fluorescence microscope (Eclipse E600 with fluorescence attachment, Nikon, Tokyo, Japan) or confocal microscope (FV 1000, Olympus, Tokyo, Japan).

For double labeling of JN and F-actin, the protocol was similar to the above except that the sections/cell cultures were incubated only in rabbit anti-JN or anti-FLAG tag primary antibody followed by goat-anti-rabbit IgG-Alexa Fluor 488 secondary antibody that yielded green fluorescence in the corresponding JN positive cells. The sections/cell culture preparations were subsequently stained for 30 min at room temperature with rhodamine-conjugated phalloidin (100 nM in PBS) that bound specifically with high affinity to F-actin, and yielded red fluorescence. After DAPI counterstaining of cell nuclei and PBS washes, the sections/cell cultures were cover-slipped and viewed under a fluorescence microscope or a confocal microscope.

2.6 | Immuno-electron microscopy

Two rats were euthanized with Numbutal (see above), and transcardially perfused with saline, followed by freshly prepared fixative solution (3% paraformaldehyde, 0.1% glutaraldehyde in 0.1 M PB, pH 7.4). The eye balls were then enucleated, and post-fixed for 2 hr in the same fixative. Vibratome sections of 100-μm thickness were prepared. Pre-embedding immuno-electron microscopy (immuno-EM) using the avidin-biotinylated horseradish peroxidase complex (ABC) kit (Vector Laboratories, Burlingame, CA) was performed on the free-floating vibratome sections (Tang et al., 2009). Briefly, the tissue sections were pre-treated with 0.3% H_2O_2 (in PBS) to quench endogenous peroxidases, and then incubated in PBS-NGS (6%) for 90 min to block non-specific binding. This was followed by an overnight incubation at room temperature in rabbit antiserum against JN diluted in PBS-NGS. Control sections were incubated in parallel in the same dilution buffer without the primary antibody. After extensive washing in PBS, the sections were incubated in biotinylated goat anti-rabbit IgG (1:200, RRID: AB_2336810) for 1.5 hr at room temperature. The avidin-biotinylated horseradish peroxidase complex (ABC) solution was prepared and then incubated with the sections according to the manufacturer's instruction. Immunoreactivity was visualized by H_2O_2 (0.01%) and diaminobenzidine tetrahydrochloride (DAB·4HCl, 0.05%). The tissue sections were post-fixed in osmium tetroxide, and further processed for electron microscopy. Semithin sections of the preparations were counterstained by using 1% toluidine blue O and observed under a light microscope. Ultrathin sections were observed under a transmission electron microscope (EM 208S, FEI, Eindhoven, the Netherlands).

2.7 | Data analysis

Quantitative analysis of cell size and F-actin binding intensity (to rhodamine phalloidin) was performed on double-fluorescence photomicrographs using ImageJ software (1.47v, National Institute of Mental Health, Bethesda, MD, USA, RRID: SCR_003070). The contour of each cell in the image was defined and labeled as a region of interest (ROI) by using imageJ. The ROIs were then measured for each of the red

(ezrin or F-actin), green (FLAG tag immunoreactivity) and blue (DAPI counterstain of nucleus) channels of the RGB image. Relative optical density (ROD) of the ROIs was corrected by subtracting the background ROD of the respective image channels, and then analyzed to determine transfection, cell size and F-actin binding intensity of each cell in the image. Statistical analysis results were considered significant (*) when Student's *t*-test or one-way analysis of variance (ANOVA) gave a p-value $< .05$, highly significant (**) when a p-value $< .01$, and non-significant when a p-value $> .05$. When one-way ANOVA revealed significant difference among groups, Fisher's least significant difference (LSD) tests were performed pairwise to find out the specific groups with statistically significant differences from the others (Hayter, 1986). Details of Fisher's LSD tests have recently been described elsewhere (Liang et al., 2017).

3 | RESULTS

3.1 | JN expression in the retinal pigment epithelial cells

By fluorescence immunohistochemistry and confocal microscopy, JN expression was revealed in RPE cells. Subcellularly, JN was located in the cytoplasm, especially at the apex and the basal infolding of the epithelial cell layer, and in the apical microvilli of RPEs (Figure 1a,b). We also surveyed possible expression of a few other oligodendroglia marker proteins in the retina. Sirtuin 2 (SIRT2), an α-tubulin deacetylase preferentially expressed in oligodendroglia and myelin sheath in the CNS (Li et al., 2007), was not detected in RPE cells (Figure 1d,e). Prominent SIRT2 immunoreactivity, however, was found along the nerve fibers of the extraocular part of the optic nerve (Figure 1c), consistent with our previous report (Li et al., 2007). CNPase and MBP also did not show detectable expression in the normal rat retina (data not shown), in agreement with findings of previous studies (Ffrench-Constant, Miller, Burne, & Raff, 1988; Gao, Macklin, Gerson, & Miller, 2006; Perry & Lund, 1990). Western blot analysis of retinal lysate demonstrated JN immunoreactivity for a single band of about 41 kDa, similar to the mobility of dephosphorylated JN of the brain. Phosphorylated JN in the eye seemed not as abundant, as judged by the absence of the slower migrating band found in brain lysate (Meng et al., 2010). Ezrin immunoreactivity in the form of an approximately 81-kDa band was found in both the brain and the eye (Figure 1f).

On double fluorescence immunohistochemical preparations, JN co-localized with ezrin in the supranuclear zone and in microvilli of RPE cells (Figure 2a–c). Overlap of JN and ZO1 immunostaining could be seen at tight junctions (Figure 2d–f). The co-localization of JN and ZO1 at RPE apical junctional complexes could be more clearly visualized at the hexagonal periphery of RPE cells on flat sections of the retina (Insets in Figure 2d–f). Double labeling of JN and actin cytoskeleton (stained with rhodamine-phalloidin) revealed similarly enriched distribution of the two at the apical and basal surfaces of RPE cells, although actin cytoskeleton signal in RPE microvilli seemed relatively weak as compared to that in the nearby structures like the outer limiting membrane (Figure 2g–i).

Nerve fibers of retinal ganglion cells were immuno-positive for the neuronal markers class III β-tubulin (TuJ1 reactivity, TuJ1-r) and microtubule-associated protein 2 (MAP2) in the retina, and after exiting the eye ball (distal to the sclera) attained myelination as marked by JN and SIRT2. Thus, distributions of JN and SIRT2 in the myelin sheaths and oligodendroglia along the nerve fibers of the extraocular part of the optic nerve were similar (Figures 1c & 3b,e). In the retina, prominent TuJ1 staining was additionally seen in the ganglion cell layer and inner plexiform layer, with weaker signals in the outer plexiform and inner nuclear layers (Figure 3a). For MAP2, strong immunoreactivity was observed in the inner plexiform layer, with decreasing labeling intensity in the ganglion cell layer, outer plexiform layer, inner segment of the rods and cones and then inner and outer nuclear layers of the retina (Figure 3d). JN was absent from all layers of the neural retina except at the tips of the outer segment of the rods and cones, where JN-positive RPE microvilli interdigitate with the tips of the photoreceptor rods and cones (Figure 3a,d).

Double fluorescence immunohistochemistry revealed glial fibrillary acidic protein (GFAP, a marker protein of astrocytes) in the nerve-fiber and ganglion-cell layers, and OX42 (a marker of microglia) in the inner-plexiform, ganglion-cell and occasionally nerve-fiber layers. Both markers were not detected in RPE cells labeled by JN (Figure 3c,f).

On toluidine blue O-stained plastic semi-thin sections of the retina (from the pre-embedded immuno-EM preparations), JN immunoreactivity in the cytoplasm of the cell bodies and microvilli of the RPE was clearly visible, and similarly distributed as seen on immunofluorescence preparations under a confocal microscope, although JN in the microvilli on the semi-thin sections was not as conspicuous as seen in the immunofluorescence preparations. Semi-thin sections of the negative control group (omitting the primary antibody) showed no immuno-reactive product in the retina (Data not shown).

Under an electron microscope, JN immunohistochemical deposits were found in the cytoplasm and microvilli of RPE cells. In some immuno-EM fields of view, JN immunoreactivity spanned the entire thickness of the RPE (Figure 4a–c). Overall, relatively higher levels of JN immunoreactivity could be seen at the apices of RPE cells and at the roots of RPE microvilli (Figure 4d,e,g). In the microvilli, JN was visible among the tips of the outer segment of rod or cone photoreceptor cells. Occasionally, a fragment of the outer segment membrane stack was seen almost encircled by JN-positive RPE microvilli (Figure 4e,h,i). At the base of the RPE cells facing the Bruch's membrane and choroid, clustering of JN immunoreactivity at or near the infoldings was also occasionally observed (Figure 4f).

3.2 | Effects of JN on morphology and actin cytoskeleton organization of cultured ARPE-19 cells

In view of the extensive co-localization of JN and actin cytoskeleton in the RPE cells (Figure 2g–i) and the fact that JN is an actin cytoskeleton-binding protein, we further investigated effects of JN expression on morphology and actin cytoskeleton architecture of cultured ARPE-19 cells. No endogenous JN was detected in ARPE-19 cells (data not shown). Expression of extrinsic JN by transfection

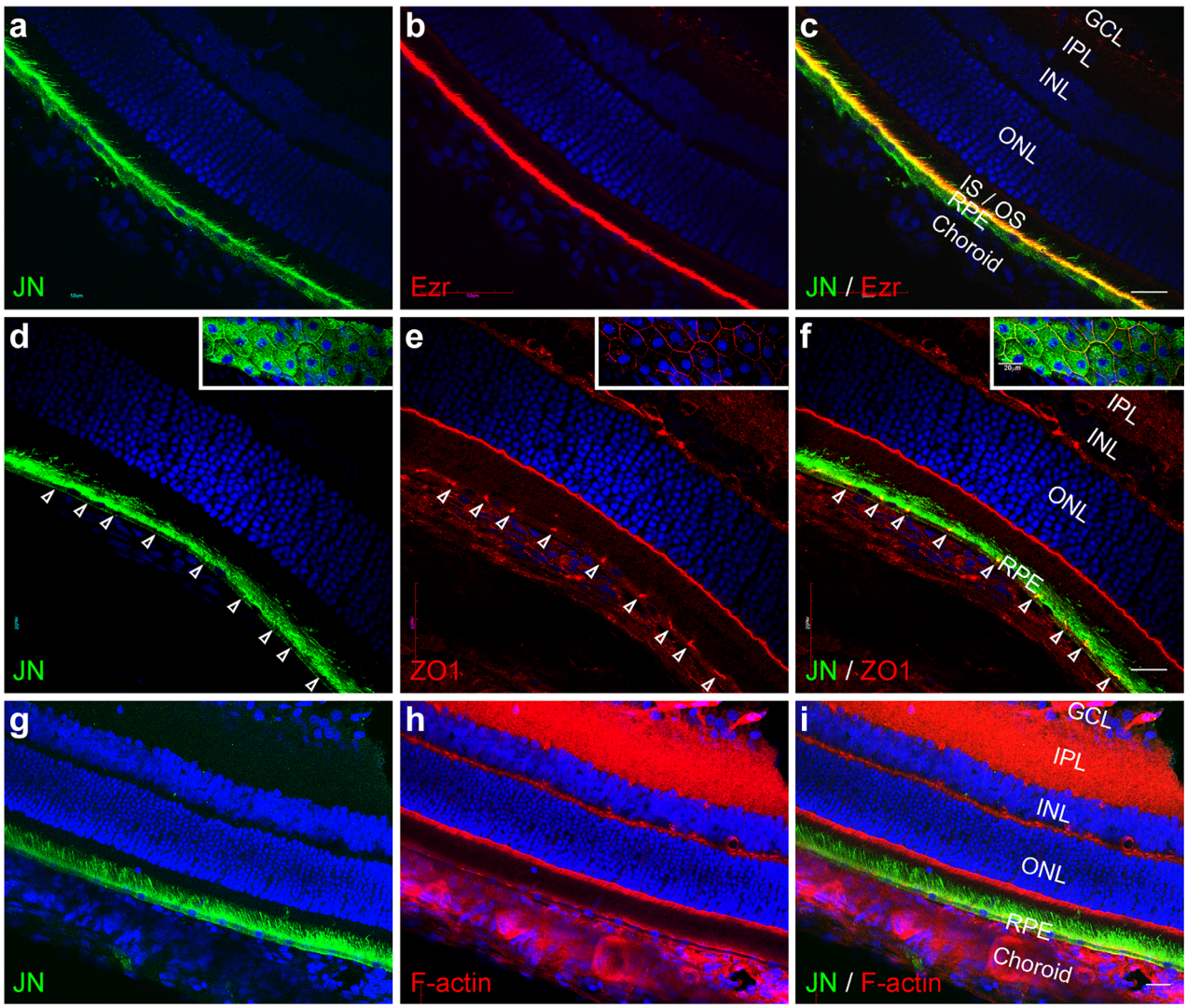

FIGURE 2 Confocal photomicrographs comparing expression/distribution of JN with that of ezrin (a–c), ZO-1 (d–f) or F-actin in the RPE cells (g–i), as revealed by double fluorescence immunohistochemistry (a–f) or JN histochemistry and F-actin binding (to phalloidin) (g–i). Note the co-localization of JN and ezrin in the supranuclear region of RPE cells (c), and partial co-localization of JN and ZO-1 at the apical junctional complexes (arrowheads in d–f) of the RPE cells. The partial co-localization of JN and ZO-1 could also be seen on flat sections of the retina (insets in d–f). JN and F-actin also mostly co-localized in the RPE cells (g–i). Abbreviations: Ezr, ezrin. For other abbreviations, see Figure 1. Scale bars, 20 μm

caused areal enlargement or spreading, but did not result in marked outgrowth of elongated cellular processes, of cultured sub-confluent ARPE-19 cells (Figure 5a–c), in contrast to the prominent JN activity in promoting ramification of cultured oligodendrocyte precursor cells (Zhang et al., 2005). Nevertheless, JN-overexpressing ARPE-19 cell did display more microvillus-like short cellular spikes as compared to the JN-141-expressing or to the unsuccessfully transfected control cells in the same culture (Figure 5a–f). Extrinsic JN in ARPE-19 cells also caused significant elevation of F-actin levels, and markedly enhanced the formation of actin cytoskeleton bundles with features similar to stress fibers. Redistribution of actin cytoskeleton bundles to the periphery of transfected cells was also observed (Figure 6a–c). Transfection with the truncated JN141 control plasmid did not induce significant changes in host cell size, arborization, or actin cytoskeleton architecture, as compared with the un-transfected cells in the same control culture (Figures 5d–f & 6d–f).

Quantitatively, areal sizes of JN-transfected ARPE-19 cells averaged 2163.33 ± 771.12 μm^2 (mean ± *SD*, analysis of 14 microscopic fields from 3 independent experiments, a total of 166 cells), whereas those of the un-transfected cells of the same experimental group measured 1369.91 ± 247.18 μm^2 (14 microscopic fields from 3 experiments, 337 cells). JN141 control plasmid transfected cells had an average areal size of 1269.30 ± 452.80 μm^2 (14 microscopic fields from 3 experiments, 202 cells), as compared to that of the un-transfected cells in the same control group (1013.76 ± 316.00 μm^2) (14 microscopic fields from 3 experiments, 490 cells). Both Student's *t*-tests and ANOVA followed by Fisher's LSD tests indicated statistically highly significant increase of JN-transfected cell size as compared to the un-transfected

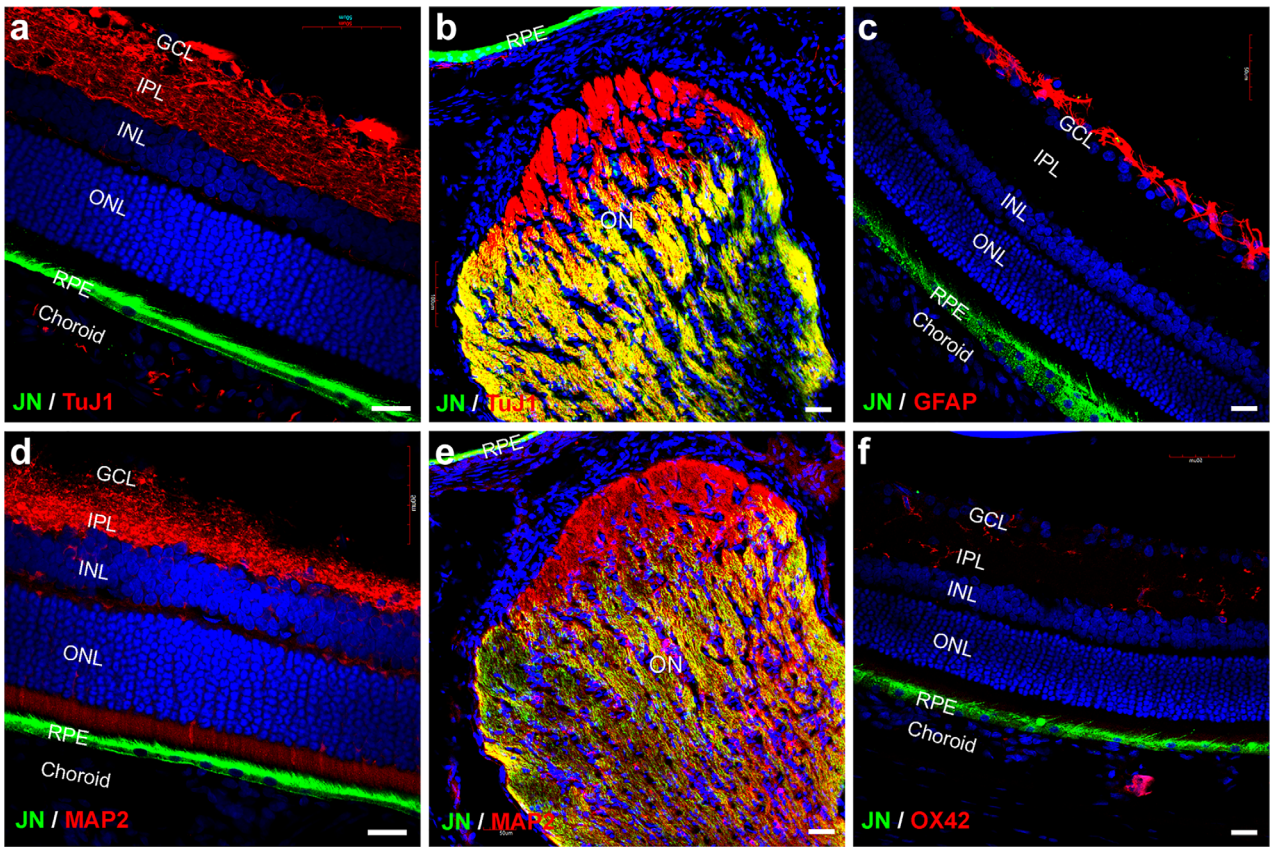

FIGURE 3 Confocal photomicrographs showing the absence of JN in neuronal cells (marked by TuJ1-r or MAP2 immunoreactivity, red in (a, b, d, e), astrocytes [marked by GFPA, red in (**c**)] and microglia [marked by OX42, red in (f)] of the retina, but presence of JN in the myelin sheaths of the extraocular optic nerve fibers (b, e). Abbreviations, ON, optic nerve. See Figure 1 for other abbreviations. Scale bars, 20 μm (a, c, d, f), 40 μm (b, e)

cells in the same experimental group, to the JN141-transfected cells of the control group, or to the JN141 unsuccessfully transfected cells of the JN141 control group ($p < .01$) (Figure 7a). Size of the JN141-transfected cells did not significantly differ from the un-transfected cells in the same microscopic fields.

Likewise, average F-actin intensity of JN-transfected cells was 0.308 ± 0.140 ROD (analysis of 9 microscopic fields from 2 independent experiments, a total of 94 cells), highly significantly higher ($p < .01$) than that of the un-transfected cells in the same microscopic fields (0.073 ± 0.040 ROD) (142 cells). JN141-transfected control cells exhibited an average F-actin binding intensity of 0.108 ± 0.049 ROD (10 microscopic fields, 2 experiments, 130 cells) that was highly significantly lower than that of the JN-transfected cells ($p < .01$), but not significantly different ($p > .05$) from that of JN141 un-transfected control cells in the same microscopic fields (0.076 ± 0.032 ROD) (311 cells) (Figure 7b).

4 | DISCUSSION

Here we report JN expression in rat RPE cells, and JN functional roles in regulating actin cytoskeleton architecture and morphology of cultured ARPE-19 cells. It is intriguing that JN, an oligodendroglia-specific protein in the CNS, is abundantly expressed in the RPE cells, whereas other oligodendroglial marker molecules such as SIRT2, CNPase and MBP are not. This situation in the RPE cells is reminiscent of that in the sustentacular cells of the olfactory neuro-epithelium, which also express JN, but not CNPase or MBP (Tang et al., 2009). RPE cells, olfactory sustentacular cells and oligodendrocytes differ greatly from one another in terms of molecular markers, morphology and functional roles. Disorders of these cell types also cause distinct pathological alterations and clinical manifestations. Yet the three JN-expressing cell types share common cell biological and functional features. For instance, they are all supporting cells to neurons, and closely associated with the supported neurons. The supporting roles of these cell types are reflected not only by wrapping, surrounding or enclosing neuronal components to structurally strengthen, separate and/or microelectrically insulate the neuronal components, but also consist of metabolic, scavenging and/or barrier support to the respective target neurons. The question is then what specific functions JN may serve in these supporting cells or in their interaction with the supported neurons or with other cellular or extracellular components.

In cultured oligodendrocyte precursor cells the biological consequences of JN modulation of actin cytoskeleton dynamics include promotion of cellular arborization, differentiation and CNPase molecular transport from the cell body to the processes (Meng et al., 2010; Zhang et al., 2005), while in the RPE cells JN mainly facilitated stress fiber

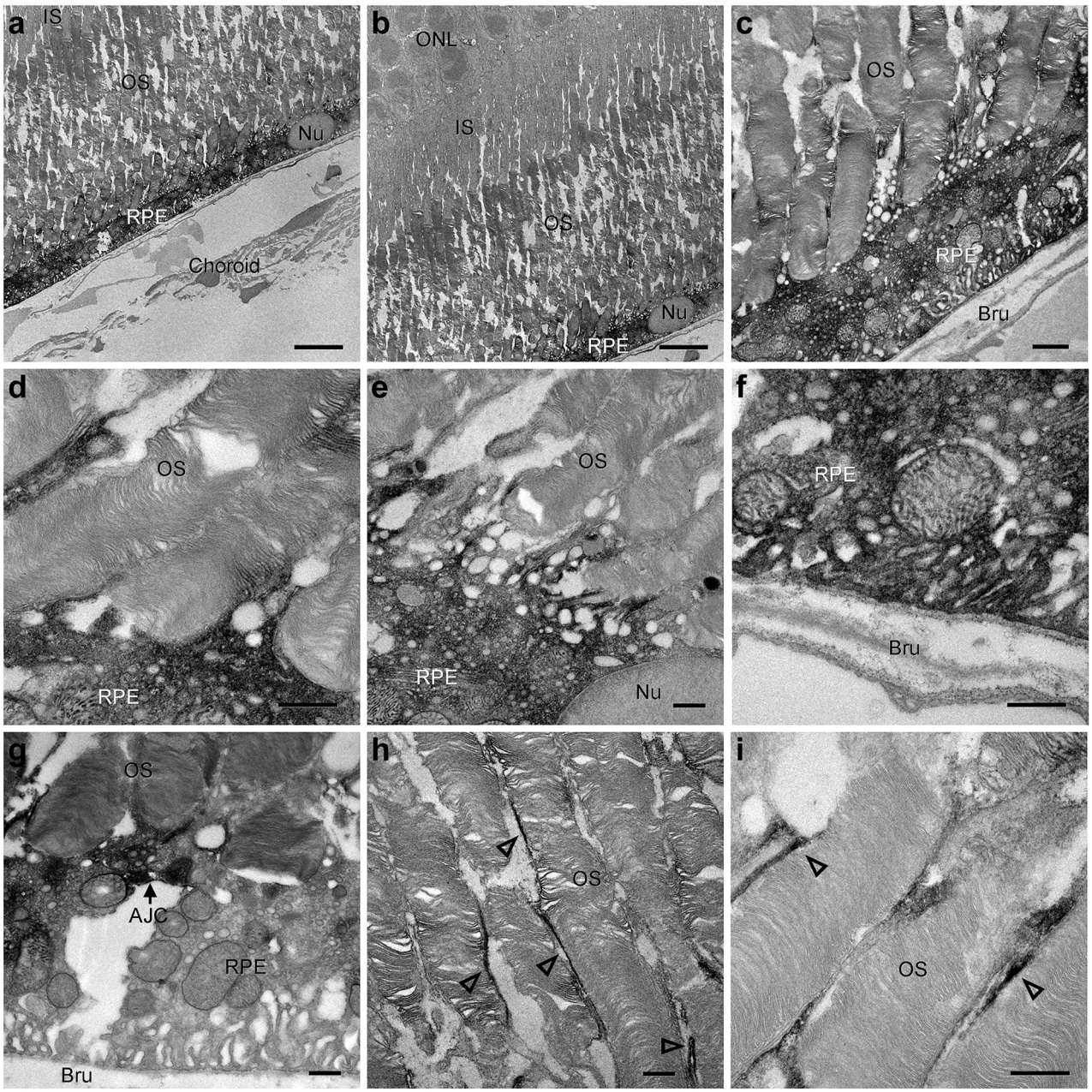

FIGURE 4 Immuno-electron microscopic photomicrographs showing expression of JN in RPE cytoplasm (a–f, g) and microvilli [arrowheads in (h, i)]. Relatively higher levels of JN immunoreactivity could be seen at the apices of RPE cells (d, e), and at near the apical junctional complex (g). Abbreviations: AJC, apical junctional complex; Bru, Bruch's membrane; Nu, nucleus. See Figure 1 for other abbreviations. Scale bars, 5 μm (a, b), 1 μm (c) or 0.5 μm (d–i)

formation and cell spreading/size expansion. JN-transfected ARPE-19 cells showed some short microvillus-like spikes, but hardly any elongated branches. The different JN activities reflect the normal morphologies and biological functions of the two respective cell types in vivo, but the molecular mechanisms underlying these differential JN effects remain unclear. Among other possibilities, variable regulatory pathways (especially the Rho GTPase pathways) and different molecular interactions of JN in the two distinct cell types may be contributing factors (Bonilha 2014; Michalski & Kothary, 2015; Nawaz et al., 2015; Zuchero et al., 2015). Phosphorylation at a specific amino acid residue, for example, down-regulates JN activity on oligodendroglial cell arborization (Meng et al., 2010). As seen from our Western blot data, the RPE cells had very low or no phosphorylated JN (Figure 1f). In addition, at the C-terminus, JN shares the F-actin binding domain of the ERM proteins, and hence might compete or synergize with other ERM molecules where they co-localize. In the case of the RPE cells, the supranuclear region and apical microvilli are sites of potential interactions among JN, ezrin, the actin cytoskeleton and related other molecules, although the exact nature and biological consequences of such interactions remain to be elucidated. Furthermore, distinct interactions

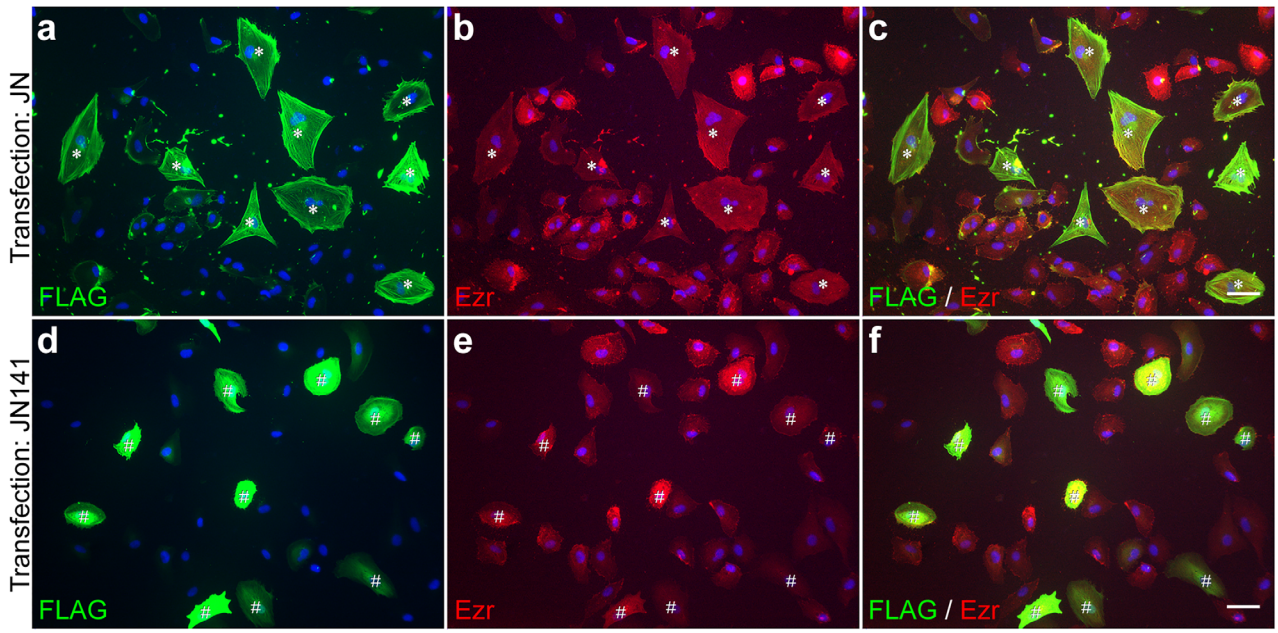

FIGURE 5 Photomicrographs showing spreading/enlargement but no elongated branches of JN-transfected ARPE-19 cells (*) in culture (a–c), as compared with neighboring un-transfected cells in the same culture or with JN141-transfected control cells (#) (d-f). Abbreviation: Ezr, ezrin; FLAG, FLAG tag. Scale bars, 50 μm

with the extracellular matrix or neighboring cells may also contribute to the different cell biological effects of JN in various cell types. Overall, it remains unclear as to what regulatory pathways for JN post-translational modification(s) are available in RPE cells or how the modification(s) may alter JN activities and binding to actin cytoskeleton.

It should be noted that the cultured ARPE-19 cells in the present study were sub-confluent and undifferentiated and only the effect of transfecting a JN or control plasmid was analyzed. It is conceivable that at higher confluency condition or other differentiation stages, ARPE-19 cell might respond differently to JN expression (Dunn, Aotaki-Keen, Putkey, & Hjelmeland, 1996; Pfeffer & Philp, 2014).

In the RPE microvilli under the confocal microscope, abundant JN-immunoreactivity was observed, but immuno-electron microscopic preparations showed relatively scarce JN signals in RPE microvilli on

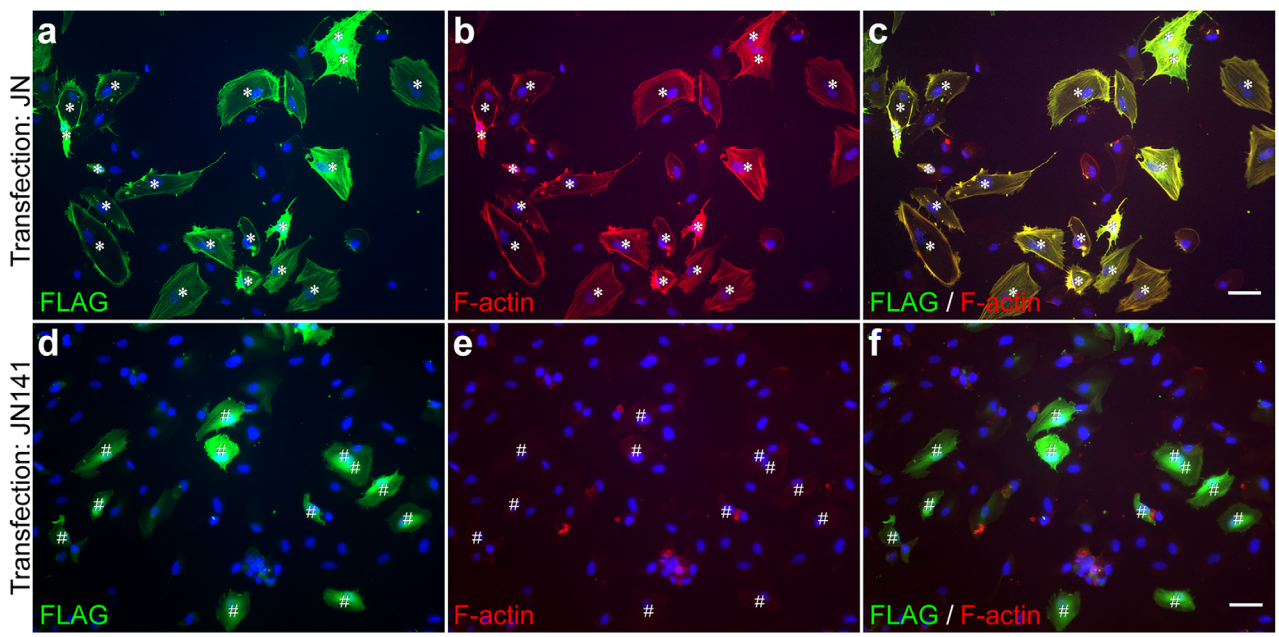

FIGURE 6 Photomicrographs showing intensification of F-actin binding and formation of stress fibers in JN-transfected ARPE-19 cells (*) in culture (a–c), as compared with neighboring un-transfected cells in the same culture or with JN141 control plasmid-transfected cells (#) (d–f). Abbreviation: FLAG, FLAG tag. Scale bars, 50 μm

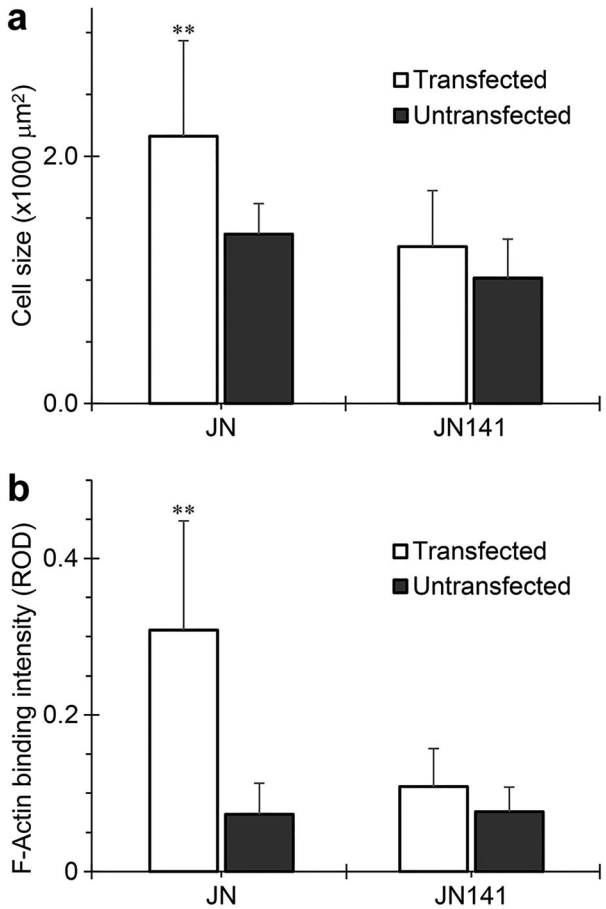

FIGURE 7 Bar graphs showing highly significant increases of cell size (a) and actin cytoskeleton binding intensity (b) in JN-transfected cells, as compared to the un-transfected cells of the same microscopic fields, to JN141-transfected cells, or to JNJ141 un-transfected cells. **, $p < .01$ (Student's *t*-tests and one-way ANOVA followed by Fisher's LSD tests)

ultra-thin sections (Figure 4). This may be partly due to the harsher tissue fixation for EM processing that could mask JN antigenicity. The ultra-thin sections (0.05–0.07 μm thick) for immuno-EM also precluded the possibility of encompassing as many RPE microvilli as the thick frozen sections (40 μm) for light microscopy. Lack of Triton X-100 in the process of the pre-embedding JN immuno-EM staining probably further limited penetration of the antibody into the depth of tissue sections, and therefore resulted in overall weaker JN signals on EM preparations.

The finding of undetectable endogenous JN in ARPE-19 cells of human origin cannot be considered definitive as the polyclonal JN antibody used in the present study was originally developed against the N-terminal 170 amino acid residues of rat JN and its reactivity to JN of human origin has not been tested. However, the absence of endogenous JN in ARPE-19 cells would be consistent with our preliminary results detecting no endogenous JN in cultured primary RPE cells of rat origin (data not shown). Cultured primary oligodendrocyte precursor cells or OLN-93 oligodendroglial cell line (both of rat origin) also did not show endogenous JN (Meng et al., 2010; Zhang et al., 2005; our unpublished data). The reason for the silencing of endogenous JN in cultured cells remains unexplained but needs to be taken into consideration when interpreting data from cultured cells.

As for SIRT2, the current study cannot rule out its expression in various cell types of the retina at levels much lower than that in the extraocular optic nerve. Our data with SIRT2 expression in the CNS indicated that while the in-house developed SIRT2 polyclonal antibody can readily detect SIRT2 in oligodendroglia/myelin sheath (Li et al., 2007), it is relatively insensitive to SIRT2 in neuronal cells as compared to a commercially available SIRT2 antibody (our unpublished observation). One possibility for this difference might be the expression of different SIRT2 splice variants in different cell types, but this assumption needs experimental validation.

As a regulator and interactive partner of the actin cytoskeleton, JN expression could have significant and far-reaching effects on diverse biological attributes and functions of cells. Here we showed JN regulation of RPE cell morphology, actin cytoskeleton abundance and organization. It remains unclear if JN also plays a role in regulating other actin cytoskeleton-related RPE structures or functions, including RPE polarity, motility, cell adhesion/junctions, intracellular or intercellular trafficking, support of photoreceptor neurons, and formation of outer blood-retina barrier. This, as well as a more detailed comparison of specific or unified functional and regulatory roles of JN in the different cell types in vitro and in vivo awaits future investigations. Last but not least, the possibility of JN expression abnormalities in retinal disorders such as proliferative vitreoretinopathy or age-related macular degeneration deserves further exploration.

ACKNOWLEDGMENTS

We are grateful to Junhong TANG for technical assistance and Yajun WU for helps with immuno-electron microscopy. This work was supported by research grants from Singapore Biomedical Research Council (BMRC/04/1/21/19/305 and 06/1/21/19/460) and MOE Academic Research Fund (AcRF R-181-000-143-112). All experiments were conducted in compliance with the ARRIVE guidelines. Preliminary results of the present study have been reported elsewhere in abstract form (Liang & Tang, 2009).

CONFLICT OF INTEREST

All authors declare that they have no conflicts of interest.

AUTHOR CONTRIBUTIONS

FYL contributed to design of study, execution of experiments and manuscript preparation. JHH and NWT did the cell culture experiments. WH contributed to manuscript preparation and revision.

ORCID

Fengyi Liang http://orcid.org/0000-0003-1162-6212

REFERENCES

Bonilha, V. L. (2014). Retinal pigment epithelium (RPE) cytoskeleton in vivo and in vitro. *Experimental Eye Research*, *126*, 38–45. https://doi.org/10.1016/j.exer.2013.09.015.

Bonilha, V. L., Finnemann, S. C., & Rodriguez-Boulan E. (1999). Ezrin promotes morphogenesis of apical microvilli and basal infoldings in retinal pigment epithelium. *Journal of Cell Biology*, *147*(7), 1533–1548.

Brockschnieder, D., Sabanay, H., Riethmacher, D., & Peles, E. (2006). Ermin, a myelinating oligodendrocyte-specific protein that regulates cell morphology. *Journal of Neuroscience*, *26*, 757–762. https://doi.org/10.1523/JNEUROSCI.4317-05.2006

Chiba, C. (2014). The retinal pigment epithelium: An important player of retinal disorders and regeneration. *Experimental Eye Research*, *123*, 107–114. https://doi.org/10.1016/j.exer.2013.07.009

Dunn, K. C., Aotaki-Keen, A. E., Putkey, F. R., & Hjelmeland, L. M. (1996). ARPE-19, a human retinal pigment epithelial cell line with differentiated properties. *Experimental Eye Research*, *62*(2), 155–169.

Ffrench-Constant, C., Miller, R. H., Burne, J. F., & Raff, M. C. (1988). Evidence that migratory oligodendrocyte-type-2 astrocyte (O-2A) progenitor cells are kept out of the rat retina by a barrier at the eye-end of the optic nerve. *Journal of Neurocytology*, *17*, 13–25.

Gao, L., Macklin, W., Gerson, J., & Miller, R. H. (2006). Intrinsic and extrinsic inhibition of oligodendrocyte development by rat retina. *Developmental Biology*, *290*, 277–286. https://doi.org/10.1016/j.ydbio.2005.11.007

Hayter A. J. (1986). The maximum familywise error rate of Fisher's least significant difference test. *Journal the American Statistical Association*, *81*(396), 1000–1004. DOI: 10.1080/01621459.1986.10478364

Li, W. B., Zhang, B., Tang, J., Cao, Q., Wu, Y., Wu, C., … Liang, F. (2007). Sirtuin 2, a mammalian homolog of yeast SIR2 longevity regulator, is an oligodendroglial protein that decelerates cell differentiation through deacetylating alpha-tubulin. *Journal of Neuroscience*, *27*, 2606–2616. https://doi.org/10.1523/JNEUROSCI.4181-06.2007

Liang, F., & Tang, J. (2009). Specific expression of juxtanodin in retinal pigment epithelial cells of the rat. *Society Neuroscience 39th Annual Meeting Abstract Online*, Program # 724.12, Chicago, IL, USA, Oct 17–21. http://www.abstractsonline.com/plan/AdvancedSearch.aspx

Liang, F., Wang, X., Ow, S. H., Chen, W., & Ong, W. C. (2017). Sirtuin 5 is anti-apoptotic and anti-oxidative in cultured SH-EP neuroblastoma cells. *Neurotoxicity Research*, *31*, 63–76. https://doi.org/10.1007/s12640-016-9664-y

Manser, E., Huang, H. Y., Loo, T. H., Chen, X. Q., Dong, J. M., Leung, T., & Lim, L. (1997). Expression of constitutively active alpha-PAK reveals effects of the kinase on actin and focal complexes. *Molecular Cell Biology*, *17*, 1129–1143.

Meng, J., Xia, W., Tang, J., Tang, B. L., & Liang, F. (2010). Dephosphorylation-dependent inhibitory activity of juxtanodin on filamentous actin disassembly. *Journal of Biological Chemistry*, *285*, 28838–28849. https://doi.org/10.1074/jbc.M110.117887

Michalski, J. P., & Kothary, R. (2015). Oligodendrocytes in a nutshell. *Frontiers in Cellular Neuroscience*, *9*, 340. https://doi.org/10.3389/fncel.2015.00340

Nawaz, S., Sánchez, P., Schmitt, S., Snaidero, N., Mitkovski, M., Velte, C., … Simons, M. (2015). Actin filament turnover drives leading edge growth during myelin sheath formation in the central nervous system. *Developmental Cell*, *34*, 139–151. https://doi.org/10.1016/j.devcel.2015.05.013

Pfeffer, B. A., & Philp, N. J. (2014). Cell culture of retinal pigment epithelium: Special Issue. *Experimental Eye Research*, *126*, 1–4. https://doi.org/10.1016/j.exer.2014.07.010.

Perry, V. H., & Lund, R. D. (1990). Evidence that the lamina cribrosa prevents intraretinal myelination of retinal ganglion cell axons. *Journal of Neurocytology 19*, 265–272.

Plafker, S. M., O'Mealey, G. B., & Szweda, L. I. (2012). Mechanisms for countering oxidative stress and damage in retinal pigment epithelium. *International Review of Cell and Molecular Biology*, *298*, 135–177. https://doi.org/10.1016/B978-0-12-394309-5.00004-3

Russo, R., Berliocchi, L., Adornetto, A., Varano, G. P., Cavaliere, F., Nucci, C., … Corasaniti, M. T. (2011). Calpain-mediated cleavage of Beclin-1 and autophagy deregulation following retinal ischemic injury in vivo. *Cell Death and Disease*, *2*, e144. https://doi.org/10.1038/cddis.2011.29.

Southwood, C. M., Peppi, M., Dryden, S., Tainsky, M. A., & Gow, A. (2007). Microtubule deacetylases, SirT2 and HDAC6, in the nervous system. *Neurochemistry Research*, *32*(2), 187–195. https://doi.org/10.1007/s11064-006-9127-6

Sparrow, J. R., Hicks, D., & Hamel, C. P. (2010). The retinal pigment epithelium in health and disease. *Current Molecular Medicine*, *10*, 802–823.

Tang, J., Tang, J. H., Ling, E. A., Wu, Y. J., & Liang, F. (2009). Juxtanodin in the rat olfactory epithelium: Specific expression in sustentacular cells and preferential subcellular positioning at the apical junctional belt. *Neuroscience 161*, 249–258. https://doi.org/10.1016/j.neuroscience.2009.03.051

Xia, W., & Liang, F. (2012). 4.1G promotes arborization and tight junction formation of oligodendrocyte cell line OLN-93. *Journal of Cell Physiology*, *227*(6), 2730–2739. https://doi.org/10.1002/jcp.23017.

Zhang, B., Cao, Q., Guo, A., Chu, H., Chan, Y. G., Buschdorf, J. P., … Liang, F. Y. (2005). Juxtanodin: An oligodendroglial protein that promotes cellular arborization and 2',3'-cyclic nucleotide-3'-phosphodiesterase trafficking. *Proceedings of the National Academy of Sciences of the United States of America*, *102*, 11527–11532. https://doi.org/10.1073/pnas.0500952102

Zuchero, J. B., Fu, M. M., Sloan, S. A., Ibrahim, A., Olson, A., Zaremba, A., … Barres, B. A. (2015). CNS myelin wrapping is driven by actin disassembly. *Developmental Cell*, *34*, 152–167. https://doi.org/10.1016/j.devcel.2015.06.011

How to cite this article: Liang F, Hwang JH, Tang NW, Hunziker W. Juxtanodin in retinal pigment epithelial cells: Expression and biological activities in regulating cell morphology and actin cytoskeleton organization. *J Comp Neurol*. 2018;526:205–215. https://doi.org/10.1002/cne.24301